

Conical Emission from Shock Waves in Ne(1–20 AGeV)+U Collisions

Philip Rau,^{1,*} Jan Steinheimer,¹ Barbara Betz,^{1,2} Hannah Petersen,^{1,3,4} Marcus Bleicher,³ and Horst Stöcker^{1,5}

¹*Institut für Theoretische Physik, Johann Wolfgang Goethe-Universität,
Max-von-Laue-Str. 1, 60438 Frankfurt am Main, Germany*

²*Department of Physics, Columbia University, 538 West 120th Street, New York, 10027, USA*

³*Frankfurt Institute for Advanced Studies (FIAS),
Ruth-Moufang-Str. 1, 60438 Frankfurt am Main, Germany*

⁴*Department of Physics, Duke University, Durham, North Carolina 27708-0305, USA*

⁵*GSI Helmholtzzentrum für Schwerionenforschung GmbH, Planckstr. 1, 64291 Darmstadt, Germany*

The formation and propagation of high-density compression waves, e.g. Mach shock waves, in cold nuclear matter is studied by simulating high-energy nucleus-nucleus collisions of Ne with U in the energy range from $E_{\text{lab}} = 0.5$ AGeV to 20 AGeV. In an ideal hydrodynamic approach, the high-density shock wave created by the small Ne nucleus passing through the heavy U nucleus is followed by a slower and more dilute Mach shock wave which causes conical emission of particles at the Mach cone angle. The conical emission originates from low-density regions with a small flow velocity comparable to the speed of sound. Moreover, it is shown that the angular distributions of emitted baryons clearly distinguish between a hydrodynamic approach and binary cascade processes used in the Ultra-relativistic Quantum Molecular Dynamics (UrQMD) transport model.

I. INTRODUCTION

Hydrodynamic models predict a sideward emission of nuclear matter in fast nucleus-nucleus collisions due to the transformation of kinetic energy of the projectile into compression and heat energy of the medium. High-density shock waves created during the collision of unequal nuclei push matter in transverse direction, generating a measurable preferential emission at a well-defined Mach angle [1–6]. This angle is connected to the medium properties, in particular to the velocity of sound

$$c_s^2 = \partial p / \partial e, \quad (1)$$

by the classical Mach cone formula

$$\theta_{\text{MC}} = \cos^{-1}(c_s/v_{\text{sh}}). \quad (2)$$

Here, v_{sh} denotes the velocity of the leading head shock wave traveling through the target nucleus.

In recent years, the investigation of (Mach) shock waves has regained tremendous attention, both on the theoretical [7–19] as well as on the experimental side [20–28], considering shock waves from partonic projectiles.

In this paper, we return to the original idea and re-investigate the creation of Mach-like shock waves as well as the sideward deflection of matter in asymmetric nucleus-nucleus collisions using (3+1)-dimensional ideal hydrodynamics [29] and the Ultra-relativistic Quantum Molecular Dynamics (UrQMD) transport model [30, 31]. The conical emission at Mach angles θ_{MC} (where θ denotes the polar angle between the beam axis and the flux of matter) persists over a wide range of beam energies and impact parameters, allowing for a comprehensive study even at lower beam energies. We analyze the change of

the particle emission angle θ_{lab} with increasing impact parameter and show the dependence of the Mach shock wave on the size of the projectile nucleus.

The (3+1)-dimensional ideal hydrodynamic calculations are performed for central and non-central Ne+U collisions at 0.5–20 AGeV, applying a chiral hadronic equation of state (EoS) that exhibits a phase transition to a chirally restored phase, as it is expected by lattice calculations [32–34]. Therefore, we are able to investigate the impact of this phase transition on the emission angle of particles from Mach-like shock waves in heavy ion collisions.

Additionally, analogous calculations are performed using the UrQMD transport model. The comparison of the different models with experimental data will allow to draw conclusions about the underlying process of the conical emission. While the conical emission of the reaction products in hydrodynamics is due to the formation of shock waves in the nuclear matter, the emission pattern in the UrQMD model is generated by binary collisions and does not show a Mach cone pattern.

II. HYDRODYNAMICS

Each hydrodynamic simulation of a collision process is initialized when the Ne nucleus starts to penetrate the U nucleus and is performed in the rest frame of the Uranium target. The ground state energy density distribution of each nucleus is given by the Woods-Saxon form

$$e(r) = e_0 / \left[1 + e^{(r-r_0)/d} \right], \quad (3)$$

where $e_0 = 147$ MeV/fm³ denotes the ground-state energy density.

The mean radius of a nucleus of mass A is computed via $r_0 = (1.12 A^{1/3} - 0.86 A^{(-1/3)})$ fm and the surface

*Electronic address: rau@th.physik.uni-frankfurt.de

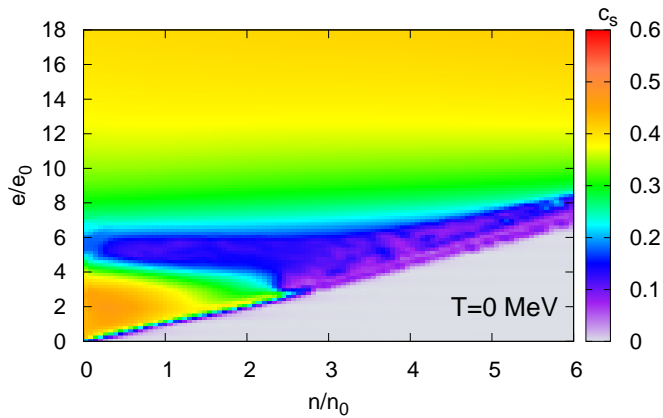


Figure 1: (Color online) The sound velocity c_s of the EoS used in our calculations as a function of e/e_0 and n/n_0 .

thickness is set to $d = 0.54$ fm [35]. In the longitudinal direction the density distribution of the projectile is Lorentz contracted. The distribution of the net baryon number density in the cold nuclei is computed accordingly with $n_0 = 0.16$ fm $^{-3}$.

Ideal hydrodynamics denotes the conservation of energy, momentum, and net baryon number

$$\begin{aligned}\partial_\mu T^{\mu\nu} &= 0, \\ \partial_\mu (nu^\mu) &= 0.\end{aligned}\quad (4)$$

These equations are numerically solved by the SHASTA algorithm [29, 36–39] on a discretized grid with the ideal hydrodynamic energy-momentum tensor given by $T^{\mu\nu} = (e+p)u^\mu u^\nu - pg^{\mu\nu}$ (with the four-velocity of the fluid $u^\mu = \gamma(1, \mathbf{v})$, $\gamma = (1-v^2)^{-1/2}$, and the net baryon density n). The algorithm ensures the flux-corrected transport of the thermodynamic quantities over the computational grid as described in Refs. [36–38]. The symmetric Eulerian grid is fixed in the target (computational) frame with a static cell size $\Delta x = 0.2$ fm. Time steps are set to $\Delta t = 0.08$ fm. Changing these numbers does not significantly affect the results.

The pressure p is connected to the energy density e and the net baryon number density n by the EoS $p(e, n)$. For this study a hadronic EoS, derived from a chiral hadronic SU(3) Lagrangian which includes the lowest baryon octet together with the multiplets of scalar, pseudo-scalar, vector, and axial-vector mesons, is used [40]. All parameters of the model EoS are fixed either by symmetry relations, hadronic vacuum observables or nuclear matter saturation properties. The model exhibits a smooth decrease of the chiral condensates (cross over) for high temperature and low baryonic potential [41, 42]. In addition, the model also provides a satisfactory description of realistic (finite-size and isospin asymmetric) nuclei and of neutron stars [41, 43, 44]. Additional baryonic degrees of freedom change the smooth cross over into a first-order phase transition with a critical end point (CEP) at $T \simeq 180$ MeV, $\mu_q \simeq 115$ MeV, depending on the couplings [40, 42, 45–47]. These values for the CEP

are within the range expected from lattice QCD calculations [32–34, 48]. For a detailed discussion of this EoS see Refs. [40, 47]. The velocity of sound c_s in the n - e -plane of this EoS is depicted in Fig. 1.

As the projectile nucleus hits the target with supersonic velocity, the nuclear matter in the collision zone gets highly compressed and thereby creates a strong shock wave that moves with $v_{\text{sh}} \geq c_s$ through the target nucleus. The shock velocity

$$v_{\text{sh}} = \left[\frac{(p_2 - p_1)(e_1 + p_2)}{(e_2 - e_1)(e_1 + p_1)} \right]^{1/2} \quad (5)$$

can be derived from the one-dimensional relativistic shock adiabat (*Taub adiabat* [49]). Quantities with index 1 denote the unperturbed nuclear matter while the index 2 denotes the energy and pressure in the compression zone. Unlike the Glassgold-Heckroth-Watson approach [50] and the participant-spectator model [51], in head-on collisions the evolving violent shock wave completely destroys the entire target nucleus, leaving no target fragments in the target frame at all. The very hot, dense, and fast moving region near the collision axis is commonly referred to as *head shock* [1, 3, 5, 16]. The center of the head shock reaches the following maximal local rest frame (lrf) energy and baryon number densities during the early evolution of the shock wave

beam energy: E_{lab} [AGeV]	0.5	1	10	20
e_{max}/e_0 (lrf)	3.5	13	32	50
n_{max}/n_0 (lrf)	3	10	11	11.

The further evolution is accompanied by a flow of energy to the outer regions of the system. This causes a significant weakening of the head shock. For beam energies $E_{\text{lab}} \geq 1$ AGeV the chirally restored phase is reached in the head shock. At the back of the shock wave, a slowly propagating region ($v \sim c_s$) with low energy density is formed. In the head shock, matter is pushed ahead while it gets deflected sideways in the outer regions of the shock wave, leading to a Mach shock structure in the medium [2, 3].

Figure 2 shows the distribution of the laboratory frame energy density e_{lab} in the reaction plane at different stages of a non-central ($b = 7$ fm) collision of Ne+U at $E_{\text{lab}} = 10$ AGeV. The upper panel displays the collision process in hydrodynamics, the lower panel in the UrQMD framework. In hydrodynamics, the evolving shock wave is clearly visible. Note that the laboratory energy density is cut off at 7 GeV/fm 3 in this figure.

The described shock wave creation is comparable to the scenario of a fast parton jet which distributes energy and momentum to the medium [7–19]. Particles emitted directly from the head shock have large momenta in forward direction and therefore are emitted at small θ_{lab} angles, while particles emitted from outer regions of the (Mach) shock wave have low momenta and are predominantly emitted in sideward directions.

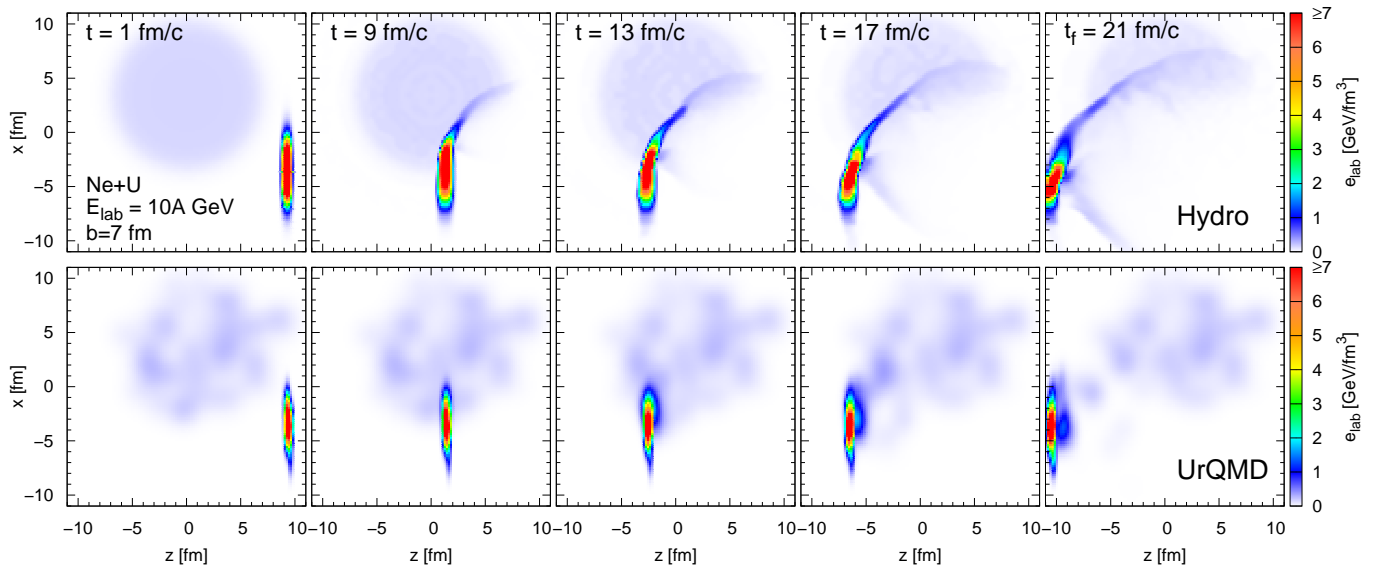


Figure 2: (Color online) Laboratory energy density (e_{lab}) distribution in the reaction plane at different stages of a Ne+U collision at $E_{\text{lab}} = 10$ AGeV and $b = 7$ fm, calculated using the hydrodynamic (upper panel) and the UrQMD framework (lower panel) from initial to final state. Note that in this plot the laboratory energy density is cut off at 7 GeV/fm^3 .

The hydrodynamic evolution is stopped at time t_f . Here, t_f is chosen large enough to ensure the full transition of the head shock through the target nucleus. The energy density distribution in the reaction plane in this final state t_f is shown in Fig. 3 for central Ne+U collisions at different beam energies, calculated using the hydrodynamic approach. The shock wave becomes stronger with increasing beam energy and thus increasing energy density in the head shock. In fact, the energy density reaches values up to $e_{\text{lab}} = 11 \text{ GeV/fm}^3$ at t_f for the highest beam energy of $E_{\text{lab}} = 20$ AGeV (cf. Fig. 3). Thus, the velocity of the head shock comes close to $v_{\text{sh}} = 1$ according to Eq. (5).

The decoupling of the hydrodynamic system into particles is done at t_f performing an isochronous freeze-out. In a first scenario, we consider a *free streaming freeze-out* (FS FO). This is a rough approximation for the distribution of light (He) and intermediate mass (Li, Be) reaction products which exhibit much less ($\sim 1/A$) thermal smearing than nucleons [2, 3]. The spectra of the reaction products are obtained by computing the relativistic kinetic energy of the nucleons from every cell on the computational grid (i, j, k) via

$$E_{\text{kin}}^{i,j,k} = (\gamma^{i,j,k} - 1) n^{i,j,k} M_N \quad (6)$$

with a nucleon mass of $M_N = 939 \text{ MeV}$ and the Lorentz gamma factor

$$\gamma^{i,j,k} = \left[1 - (v_z^{i,j,k})^2 \right]^{-1/2}, \quad (7)$$

where $v_z^{i,j,k}$ denotes the velocity and $n^{i,j,k}$ the net baryon density of the specific fluid element. The polar angle

between the matter flux and the beam axis

$$\theta_{\text{lab}} = \cos^{-1} \left(\frac{v_z^{i,j,k}}{|v^{i,j,k}|} \right) \quad (8)$$

is computed for each cell and all baryons on the grid. I.e., thermal smearing and resonance decays are neglected in this scenario.

A second freeze-out scenario is the Cooper-Frye prescription [52] (CF FO)

$$E \frac{dN}{d^3p} = \int d\sigma_\mu p^\mu f(x, p), \quad (9)$$

where $f(x, p)$ denotes the boosted distribution function and $d\sigma_\mu = (d^3x, \mathbf{0})$ the normal vector on the hypersurface. We will consider the Cooper-Frye freeze-out with and without final state interactions and resonance decays which are performed using the UrQMD model as an afterburner. The details about performing this Cooper-Frye freeze-out after the hydrodynamic evolution as well as the integration into the UrQMD model are described in detail in Ref. [53]. The hydrodynamic calculations are contrasted with simulations within a binary collision hadronic cascade, the default UrQMD model without a hydrodynamic phase [30, 31]. In the latter two approaches the emission angle of the baryons with respect to the beam axis is computed via $\theta_{\text{lab}} = \cos^{-1}(p_z/|p|)$.

The hydrodynamic calculations show a sizeable fraction of particles with low kinetic energies. They are emitted from regions with low flow velocities behind the leading head shock at angles in the range of θ_{MC} (Eq. (2)). In contrast, particles with high kinetic energies stemming from the highly compressed head shock should be emitted under small angles. Since the head shock gets remarkably stronger with increasing beam energy, an increasing

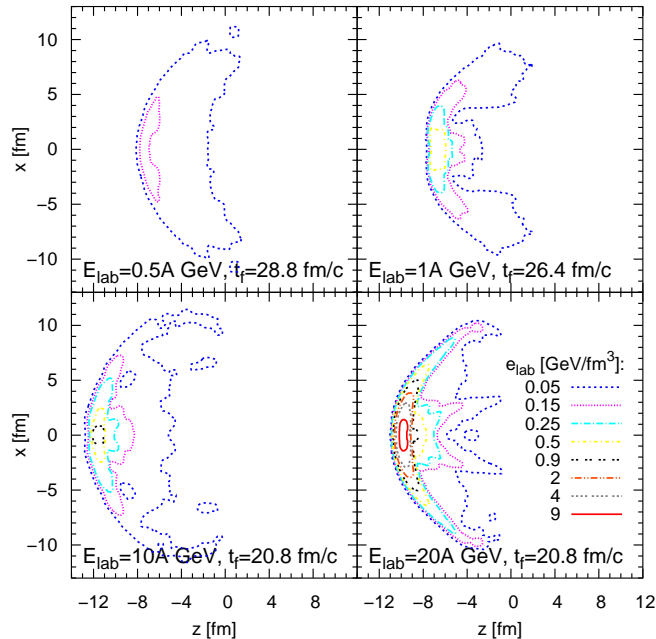


Figure 3: (Color online) Laboratory frame energy density e_{lab} [GeV/fm^3] distribution in the reaction plane at t_f , i.e. when the head shock wave has passed through the target nucleus, calculated in a hydrodynamic approach. The maximum energy density in the center of the head shock is $e_{\text{lab}} \approx 0.2, 1.6, 2, 11 \text{ GeV}/\text{fm}^3$ for projectile energies of $E_{\text{lab}} = 0.5, 1, 10, 20 \text{ AGeV}$.

number of high energetic particles is expected at small angles and higher beam energies.

III. RESULTS AND DISCUSSION

Figure 4 shows the kinetic energy distributions of nucleons, obtained with the free streaming freeze-out, for different beam energies. Beam energies in the range of $E_{\text{lab}} \leq 10 \text{ AGeV}$ show a distinct peak for nucleons with low kinetic energies ($E_{\text{kin}} \leq 50 \text{ MeV}$). For higher beam energies, however, the peak height decreases, but due to the creation of a stronger head shock more particles are produced at higher E_{kin} .

This strong head shock, leading to a particle emission in forward direction, can clearly be seen from the angular distribution of the emitted nucleons in the uppermost panel of Fig. 5, where the hydrodynamic scenario was applied, followed by the free streaming freeze-out. While one clearly observes the suppression of particle emission under small angles for $E_{\text{lab}} \leq 10 \text{ AGeV}$, a strong head shock develops at higher beam energies and pushes a considerable amount of matter ahead, resulting in a particle emission at small angles ($\theta_{\text{lab}} < 20^\circ$) and a reduced emission of particles in θ_{MC} -direction. However, for all beam energies investigated in this study, a considerable number of nucleons is emitted at large angles ($50^\circ < \theta_{\text{lab}} < 80^\circ$) due to the sideward deflection of matter in the evolving

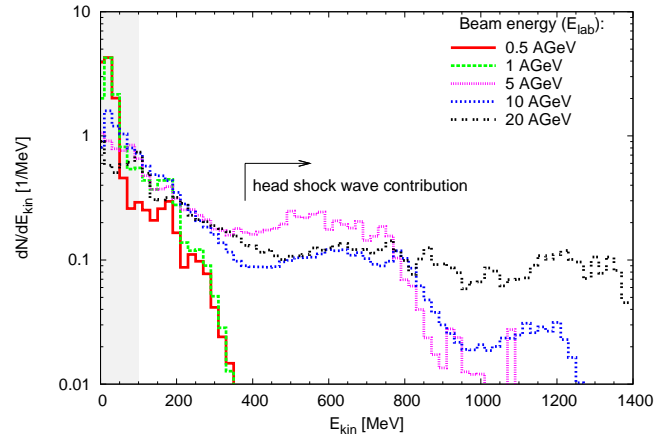


Figure 4: (Color online) Energy spectra of reaction products in Ne+U collisions. The majority of nucleons at the Mach angle arises from the low-energy (shaded) region $E_{\text{kin}} \leq 100 \text{ MeV}$, corresponding to a nucleon velocity $v = 0.43$. High-energy particles, however result from head shock regions.

Mach shock wave.

The two middle panels in Fig. 5 show results from hydrodynamic calculations with particle production via the Cooper-Frye freeze-out (second panel from top) and subsequently the UrQMD afterburner (third panel). The maxima of the distributions θ_{max} are now located at much smaller angles within a range $20^\circ < \theta_{\text{lab}} < 50^\circ$. Here, the fully isotropic, but Lorentz-boosted thermal particle distribution considered in the Cooper-Frye freeze-out [53] is superimposed on the results from the hydrodynamic calculations.

To understand this result one can consider a simple toy model where a significantly strong isotropic particle distribution, boosted in beam direction, is superimposed on the results from pure hydrodynamics. This simple approach can reproduce the effect of the Cooper-Frye freeze-out on the particle distribution. Note, that due to reasons of geometry, a fully isotropic (thermal) distribution has a $\sin(\theta)$ -shape in the comoving frame when plotted as $dN/d\theta$. If this distribution is moving with respect to the observer (laboratory frame) the sinusoidal shape is deformed and the maximum of the distribution is shifted to smaller angles.

Particle rescattering and the decay of baryonic resonances within the UrQMD afterburner, however, shift the maxima of the angular distribution of emitted nucleons to slightly larger angles (cf. third panel of Fig. 5).

The lowest panel of Fig. 5 shows the results of default UrQMD calculations. The momentum conserving particle scattering results in much broader and smoother angular distributions, with maxima about $30^\circ < \theta_{\text{lab}} < 70^\circ$, dependent on the beam energy. The shape of the curves simply reflects an isotropic distribution that is Lorentz-boosted with a certain velocity on top of the fermi distributed nucleons which did not interact at all.

Figure 6 illustrates that a cut in the kinetic energy

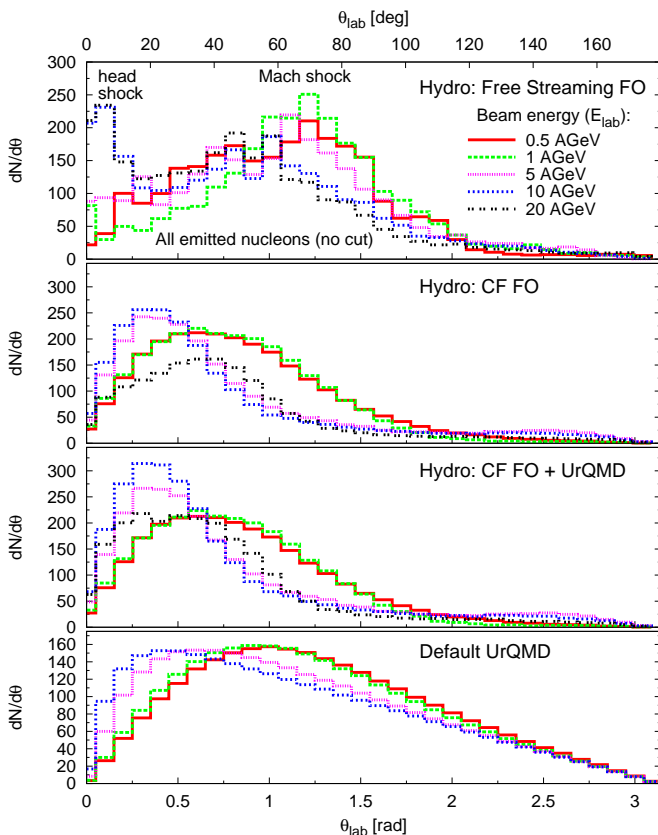


Figure 5: (Color online) Angular distributions of nucleons obtained from Ne+U reactions calculated using the hydrodynamic approach with the free streaming freeze-out (upper panel), the Cooper-Frye freeze-out (upper middle panel) and the Cooper-Frye freeze-out with the UrQMD afterburner (lower middle panel). The lowermost panel shows results from default UrQMD calculations without a hydrodynamic phase.

per nucleon at roughly the speed of sound, which corresponds to an $E_{\text{kin}} \leq 100$ MeV, changes the angular distribution for all scenarios, in particular for the higher beam energies ($E_{\text{lab}} > 1$ AGeV). The high-energetic particles predominantly originate from hot and dense regions of the head shock which is explicitly excluded by the application of this cut. Therefore, only particles emitted from the much cooler and more dilute sideways traveling Mach shock wave are observed in this analysis. For the UrQMD calculations this cut removes most forward moving participant nucleons and leaves mostly the fermi distributed spectators in the spectrum.

Plotting $dN/d\cos\theta$ instead eliminates the sinusoidal shape as can be seen in Fig. 7. Here, the Cooper-Frye freeze-out shows a clear peak at very small angles for lower beam energies ($E_{\text{kin}} \leq 100$ MeV) due to the head shock wave and the superimposed thermal distribution similar to the one seen in the lowest panel. The results from the free streaming freeze-out (uppermost panel) and with this the Mach shock wave signal is the less affected by this change.

Figure 8 depicts the dependence of the conical emission

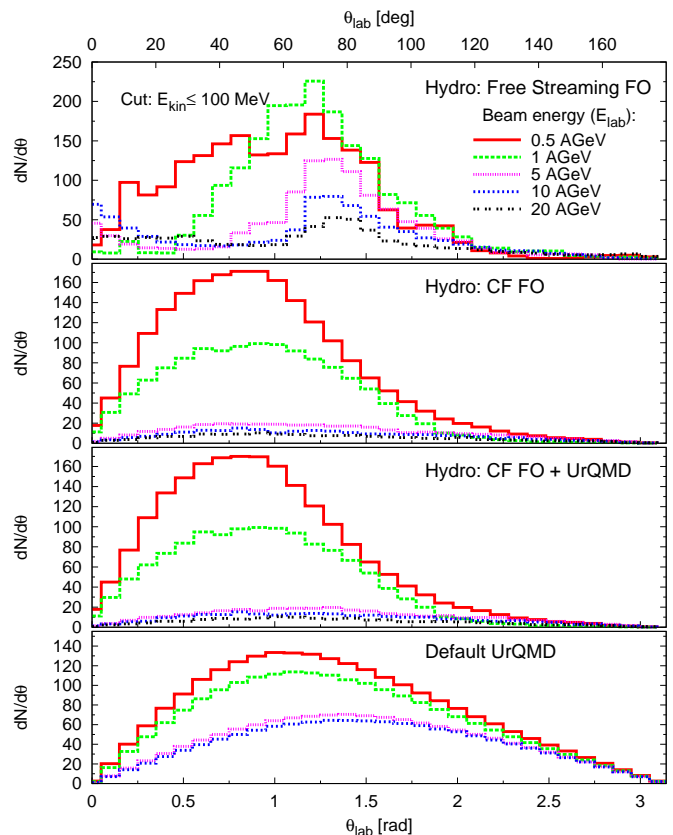


Figure 6: (Color online) Angular distributions of low energy reaction products ($E_{\text{kin}} \leq 100$ MeV) of Ne+U reactions calculated using the hydrodynamic approach with the free streaming freeze-out (upper panel), the Cooper-Frye freeze-out (upper middle panel) and the Cooper-Frye freeze-out with the UrQMD afterburner (lower middle panel). They show emission at distinct Mach cone angles in the investigated scenarios (cf. Fig. 5). The maxima of these distributions θ_{max} for the different scenarios are depicted in Fig. 8.

angle θ_{max} on the beam energy, for the different freeze-out descriptions considered. The angles are extracted from the underlying data of Fig. 6 which includes a low-energy cut so that only particles with $E_{\text{kin}} \leq 100$ MeV are considered that originate predominantly from dilute and slow fluid cells, i.e. the Mach shock wave. Those did not cross the phase transition to the chirally restored phase. Therefore, the resulting particle emission at Mach angles is probing the purely hadronic phase. It is obvious that the Mach wave travels with $v \simeq c_s$ through the hadronic phase which should result in a rather slight change of the emission angle with varying beam energy.

For the free streaming freeze-out (full triangles), the emission angle grows slightly with increasing beam energy. For the Cooper-Frye freeze-out disregarding the subsequent resonance decays (open squares) however, the emission angle is notably shifted towards smaller values due to the superimposition of the boosted thermal distribution. By employing the UrQMD-afterburner (full squares), the computed preferential emission angle gets

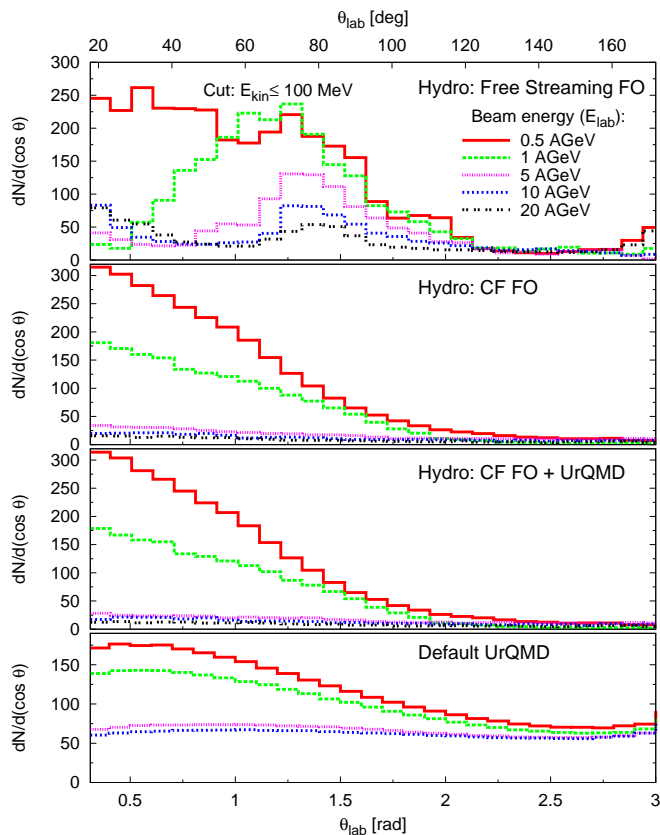


Figure 7: (Color online) Angular distribution of low energy re-action products (Fig. 6) of Ne+U reactions calculated using the hydrodynamic approach with the free streaming freeze-out (upper panel), the Cooper-Frye freeze-out (upper middle panel), the Cooper-Frye freeze-out with the UrQMD afterburner (lower middle panel), and default UrQMD (lowermost panel), from which the $\sin(\theta)$ -shape of an isotropic thermal particle distribution was removed by plotting $dN/d\cos(\theta)$.

shifted by about $\Delta\theta_{\text{lab}} = +10^\circ$.

Most of the cluster-bound particles from hydrodynamics with free streaming freeze-out are emitted at Mach angles within the range $70^\circ < \theta_{\text{MC}} < 80^\circ$ for $E_{\text{lab}} > 1$ AGeV [54]. This result corresponds to a *cluster flow* with the speed of sound.

Comparing the results obtained from the purely hydrodynamic calculations to the results from the hadronic transport model calculations without a hydrodynamic phase (UrQMD, full circles in Fig. 8) shows that even the pure transport calculation suggests conical emission of nucleons, at angles very similar to the expected Mach cone angles (note that, for the UrQMD results, the same cut in kinetic energy of the nucleons is applied). While in the hydrodynamic picture the conical emission originates from a Mach-like wave, binary nucleon-nucleon scattering results in the distinct particle emission pattern in the transport model which approximates the shape of a boosted thermal distribution.

It is possible to distinguish those scenarios by determining the predominant cluster emission angle at non-

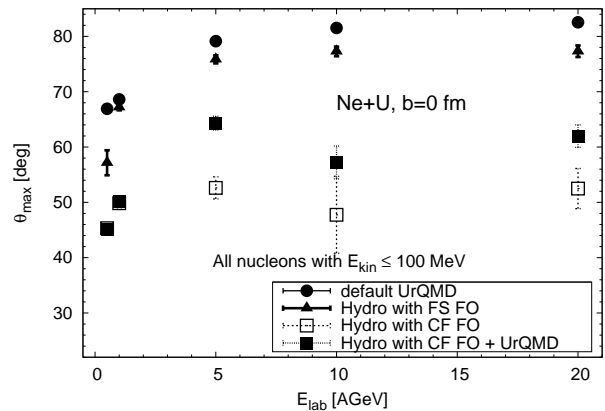


Figure 8: Beam energy dependence of the emission angle θ_{max} for default UrQMD (full circles) and hydrodynamic processes, including the free streaming freeze-out (full triangles), the Cooper-Frye freeze-out with (full squares) and without (open squares) a subsequent UrQMD afterburner.

vanishing impact parameters. The left panel of Fig. 9 shows non-central Ne+U collisions at $E_{\text{lab}} = 5$ AGeV for hydrodynamic calculations followed by the free streaming freeze-out as well as default UrQMD calculations. Here, only nucleons emitted within the energy range of $10 \text{ MeV} \leq E_{\text{kin}} \leq 100 \text{ MeV}$ are taken into account in order to ensure that nucleons originating from the spectator part of the target nucleus are excluded. In the hydrodynamic scenario, the extracted emission angle stays at $\theta_{\text{MC}} \simeq 77^\circ$ up to an impact parameter of $b = 4$ fm. For larger impact parameters, θ_{lab} decreases considerably to $\theta_{\text{lab}} \simeq 60^\circ$ for $b = 9$ fm. In this case, the projectile hits the target at its periphery (cf. Fig. 2) and the Mach shock wave propagates through the whole of the heavy nucleus. UrQMD calculations however, show a different behavior. Here, the extracted angle θ_{max} grows with increasing impact parameter, up to $\theta_{\text{max}} = 90^\circ$. This distribution pattern corresponds to a fully isotropic particle emission.

Thus, the emission angle for semi-central collisions can be used to study the reaction mechanism. While emission angles above $\theta_{\text{max}} \simeq 80^\circ$ favour kinetic collision processes to cause conical emission, emission angles well below this value indicate collective Mach shock waves in nuclear matter.

The right panel of Fig. 9 depicts the maximum emission angle of emitted nucleons in A+U collisions with $E_{\text{kin}} \leq 100 \text{ MeV}$. Here, the emission angle stays constant at $\theta_{\text{max}} \simeq 77^\circ$ from α up to Ca projectiles. The particle number in the low energy bin drops by about 75%, and collisions with Ag-projectiles show that there are virtually no particles with kinetic energies below 100 MeV left. The whole dense matter system formed by the two colliding nuclei merges completely into a highly accelerated shocked fireball [51]. Compared to these hydrodynamic calculations, the emission angles for A+U col-

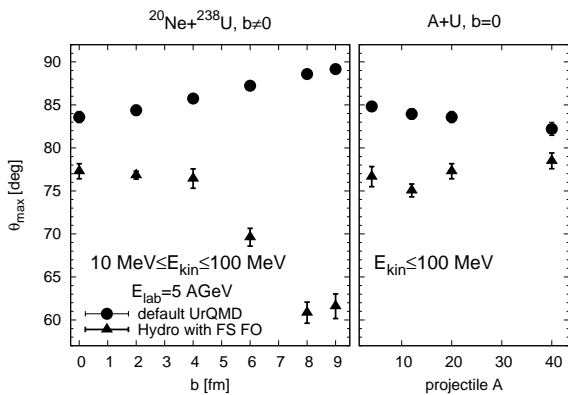


Figure 9: Maximum emission angle θ_{\max} of emitted nucleons from hydrodynamic (free-streaming freeze-out) and UrQMD calculations for non-central Ne+U collisions (left) and for central A+U collisions (right) at $E_{\text{lab}} = 5$ AGeV.

lisions computed with the default UrQMD model are larger by roughly 10° .

IV. SUMMARY

We studied the emission angles θ_{lab} (θ denotes the polar angle between the beam axis and the flux of matter) of reaction products in Ne+U collisions in a beam energy range from $E_{\text{lab}} = 0.5$ AGeV to 20 AGeV in a hydrodynamic approach with different freeze-out methods as well as using the UrQMD model. It is shown that a strong head shock wave is created during the hydrodynamic evolution due to the strong compression of nuclear matter in the collision zone. This head shock penetrates the target nucleus with a supersonic velocity v_{sh} and reaches very high energy as well as baryon densities which are sufficient to enter the chirally restored state of matter that is described by the EoS.

Behind the head shock a more dilute Mach cone like wave (*Mach shock wave*) evolves and propagates at slower velocity ($v \simeq c_s$) through the hadronic state.

We show that the energy spectra of emitted nucleons peaks at low kinetic energies (see Fig. 4). These slow particles ($E_{\text{kin}} \leq 100$ MeV) are mostly emitted at Mach angles which can be extracted from hydrodynamic calculations followed by a free streaming freeze-out (cf. Figs. 5 to 7). Those peaks should be visible even for beam energies reached at the FAIR at GSI. These rather small emis-

sion angles for all investigated beam energies lead to the conclusion that Mach-like waves travel in the hadronic phase only. Therefore, a crossing of the phase transition to the chirally restored phase as it may occur in the head shock seems not to be accessible through the emission angles of the measured particles.

Applying however a Cooper-Frye freeze-out (with and without the UrQMD afterburner), these peaks are shifted to smaller angles when plotting $dN/d\theta$ due to the superposition with the fully isotropic, but Lorentz-boosted thermal particle distribution considered in the Cooper-Frye freeze-out. Removing the sinusoidal shape of the boosted thermal distribution by considering $dN/d\cos\theta$ -distributions (see again Figs. 5 to 7), these Mach cone peaks can no longer be seen.

While results from standard UrQMD calculations lead to emission angles comparable to those of a hydrodynamic calculation followed by a Cooper-Frye freeze-out for central collisions (cf. Figs. 5 to 7), they show a notably different behavior for non-vanishing impact parameters (see Fig. 9, left panel). Thus, the emission angle can be used to distinguish the underlying process leading to a conical emission pattern of nucleons, checking the existence of shock waves in nuclear matter.

Moreover, we show that for different projectiles from α up to Ca a distinct particle emission angle prevails over a wide range of impact parameters for both hydrodynamic and UrQMD calculations (cf. Fig. 9, right panel).

V. ACKNOWLEDGEMENTS

We thank Dirk Rischke for providing the one fluid hydrodynamics code that was used for our calculations and Giorgio Torrieri for the fruitful discussions. This work was supported by GSI, BMBF, and by the Hessian LOEWE initiative through the Helmholtz International Center for FAIR (HIC for FAIR), the Helmholtz Graduate School for Heavy Ion Research, and the Helmholtz Research School on Quark Matter Studies. B.B. and H.P. acknowledge a Feodor Lynen fellowship of the Alexander von Humboldt foundation. This work was partially supported by the US-DOE Nuclear Science grant DE-FG02-93ER40764 and the U.S. department of Energy grant DE-FG02-05ER41367. We are grateful to the Center for the Scientific Computing (CSC) at Frankfurt University for providing the computational resources.

-
- [1] J. Hofmann, H. Stoecker, W. Scheid, and W. Greiner (1975), report of the Workshop on BeV/nucleon Collisions of Heavy Ions: How and Why, Bear Mountain, New York, 29 Nov - 1 Dec 1974.
 [2] H. G. Baumgardt et al., Z. Phys. **A273**, 359 (1975).
 [3] J. Hofmann, H. Stoecker, U. W. Heinz, W. Scheid, and

- W. Greiner, Phys. Rev. Lett. **36**, 88 (1976).
 [4] H. Stoecker, W. Scheid, and W. Greiner, Fizika **9**, S78(NO.2) (1977).
 [5] H. Stoecker, J. A. Maruhn, and W. Greiner, Phys. Rev. Lett. **44**, 725 (1980).
 [6] H. Stoecker et al., Phys. Rev. Lett. **47**, 1807 (1981).

- [7] H. Stoecker, Nucl. Phys. **A750**, 121 (2005).
- [8] L. M. Satarov, H. Stoecker, and I. N. Mishustin, Phys. Lett. **B627**, 64 (2005).
- [9] J. Ruppert and B. Muller, Phys. Lett. **B618**, 123 (2005).
- [10] J. Casalderrey-Solana, E. V. Shuryak, and D. Teaney, J. Phys. Conf. Ser. **27**, 22 (2005).
- [11] J. Casalderrey-Solana, E. V. Shuryak, and D. Teaney (2006), arXiv:hep-ph/0602183.
- [12] A. K. Chaudhuri and U. Heinz, Phys. Rev. Lett. **97**, 062301 (2006).
- [13] T. Renk and J. Ruppert, Phys. Rev. **C73**, 011901 (2006).
- [14] H. Stoecker, B. Betz, and P. Rau, PoS **CPOD2006**, 029 (2006).
- [15] R. B. Neufeld, B. Muller, and J. Ruppert, Phys. Rev. **C78**, 041901 (2008).
- [16] B. Betz, M. Gyulassy, J. Noronha, and G. Torrieri, Phys. Lett. **B675**, 340 (2009).
- [17] B. Betz et al., Phys. Rev. **C79**, 034902 (2009).
- [18] J. Noronha, M. Gyulassy, and G. Torrieri, Phys. Rev. Lett. **102**, 102301 (2009).
- [19] I. Bouras et al., Phys. Rev. Lett. **103**, 032301 (2009), 0902.1927.
- [20] J. Adams et al. (STAR), Phys. Rev. Lett. **95**, 152301 (2005).
- [21] S. S. Adler et al. (PHENIX), Phys. Rev. Lett. **97**, 052301 (2006).
- [22] S. S. Adler et al. (PHENIX), Phys. Rev. **C73**, 054903 (2006).
- [23] J. G. Ulery (STAR), Nucl. Phys. **A774**, 581 (2006).
- [24] N. N. Ajitanand (PHENIX), Nucl. Phys. **A783**, 519 (2007).
- [25] J. G. Ulery (STAR), Int. J. Mod. Phys. **E16**, 2005 (2007).
- [26] J. G. Ulery (2008), arXiv:0801.4904.
- [27] A. Adare et al. (PHENIX), Phys. Rev. **C78**, 014901 (2008).
- [28] B. I. Abelev et al. (STAR), Phys. Rev. Lett. **102**, 052302 (2009).
- [29] D. H. Rischke, Y. Puerstuen, J. A. Maruhn, H. Stoecker, and W. Greiner, Heavy Ion Phys. **1**, 309 (1995).
- [30] S. A. Bass et al., Prog. Part. Nucl. Phys. **41**, 255 (1998).
- [31] M. Bleicher et al., J. Phys. **G25**, 1859 (1999).
- [32] Z. Fodor and S. D. Katz, JHEP **03**, 014 (2002).
- [33] F. Karsch, J. Phys. **G31**, S633 (2005).
- [34] Z. Fodor, S. D. Katz, and C. Schmidt, JHEP **03**, 121 (2007).
- [35] H. D. Vries, C. W. D. Jager, and C. D. Vries, At. Data Nucl. Data Tables **36**, 495 (1987).
- [36] J. P. Boris and D. L. Book, J. Comput. Phys. **11**, 38 (1973).
- [37] D. L. Book, J. P. Boris, and K. Hain, J. Comput. Phys. **18**, 248 (1975).
- [38] D. H. Rischke, S. Bernard, and J. A. Maruhn, Nucl. Phys. **A595**, 346 (1995).
- [39] D. H. Rischke, Y. Puerstuen, and J. A. Maruhn, Nucl. Phys. **A595**, 383 (1995).
- [40] J. Steinheimer et al., Phys. Rev. **C77**, 034901 (2008).
- [41] P. Papazoglou et al., Phys. Rev. **C59**, 411 (1999).
- [42] D. Zschesche, S. Schramm, H. Stoecker, and W. Greiner, Phys. Rev. **C65**, 064902 (2002).
- [43] S. Schramm, Phys. Rev. **C66**, 064310 (2002).
- [44] S. Schramm, Phys. Lett. **B560**, 164 (2003).
- [45] J. Theis et al., Phys. Rev. **D28**, 2286 (1983).
- [46] D. Zschesche, G. Zeeb, S. Schramm, and H. Stoecker, J. Phys. **G31**, 935 (2005).
- [47] D. Zschesche, G. Zeeb, and S. Schramm, J. Phys. **G34**, 1665 (2007).
- [48] Z. Fodor and S. D. Katz, JHEP **04**, 050 (2004).
- [49] A. H. Taub, Phys. Rev. **74**, 328 (1948).
- [50] A. E. Glassgold, W. Heckroth, and K. M. Watson, Ann. Phys. (Paris) **6**, 1 (1959).
- [51] G. D. Westfall et al., Phys. Rev. Lett. **37**, 1202 (1976).
- [52] F. Cooper and G. Frye, Phys. Rev. D **10**, 186 (1974).
- [53] H. Petersen, J. Steinheimer, G. Burau, M. Bleicher, and H. Stoecker, Phys. Rev. **C78**, 044901 (2008).
- [54] The emission angle in events with $E_{\text{lab}} \leq 1$ AGeV is smaller than 70° because the shock wave does not exhibit such high densities and thus moves with rather low velocity only [cf. Eq. (2)].